

Revealing non-Markovian Kondo transport with waiting time distributions

Feng-Jui Chan,^{1,2,*} Po-Chen Kuo,^{1,2,*} Neill Lambert,^{3,†} Mauro Cirio,^{4,‡} and Yueh-Nan Chen^{1,2,5,§}

¹*Department of Physics, National Cheng Kung University, 701 Tainan, Taiwan*

²*Center for Quantum Frontiers of Research and Technology, NCKU, 701 Tainan, Taiwan*

³*Theoretical Quantum Physics Laboratory, Cluster for Pioneering Research, RIKEN, Wakoshi, Saitama 351-0198, Japan*

⁴*Graduate School of China Academy of Engineering Physics, Haidian District, Beijing, 100193, China*

⁵*Physics Division, National Center for Theoretical Sciences, Taipei, 106319, Taiwan*

(Dated: October 8, 2024)

We investigate non-Markovian transport dynamics and signatures of the Kondo effect in a single impurity Anderson model. The model consists of a quantum dot (QD) with ultra-strong coupling to a left lead and weak coupling to a right lead acting as a detector. We calculate the waiting time distribution (WTD) of electrons tunneling into the detector using a combination of the hierarchical equations of motion approach (HEOM) and a dressed master equation. Oscillations emerge in the short-time WTD, becoming more pronounced with stronger left-lead coupling. Fourier analysis reveals a blue shift in the oscillation frequency as coupling increases, indicating enhanced system-bath hybridization. Crucially, comparison with a dressed master equation confirms that these oscillations are a direct consequence of non-Markovian system-bath correlations. We examine the Kondo effect's influence on these oscillations by varying the quantum dot's Coulomb repulsion. Increasing this interaction enhances the WTD oscillations, coinciding with the signatures of a strengthened Kondo resonance in the quantum dot's density of states. Our results demonstrate that WTD oscillations offer a valuable tool for probing non-Markovian system-bath interactions and the emergence of Kondo correlations within quantum dot systems.

I. INTRODUCTION

Open quantum systems, where a system of interest is coupled to one or more environments, exhibit rich dynamics that often deviate from the traditional Markovian picture [1, 2]. In the Markovian approximation, the system's evolution is described by a memory-less master equation, such as the Lindblad equation [3–5]. However, this approximation breaks down when the system-environment coupling is strong or when the environmental correlation times become long, leading to non-Markovian dynamics [6–10].

Non-Markovian dynamics are characterized by the backflow of information from the environment to the system, giving rise to memory effects [11–14]. These effects play a crucial role in various quantum processes, including quantum transport in nanoscale devices [15–18]. Understanding and controlling non-Markovian effects is essential for harnessing the full potential of quantum technologies, as they can profoundly impact the coherence and entanglement properties of quantum systems [19–24].

One striking manifestation of strong system-environment coupling is the Kondo effect [25], which arises from the many-body entanglement between electrons in the system and those in the environment [26–32]. In particular, QDs have emerged as versatile platforms for engineering and probing the Kondo effect [32–38],

offering insights into the interplay between many-body physics and quantum transport [39–43].

A powerful tool for studying the influence of non-Markovian environments and the Kondo effect on quantum transport [32, 42–46] is the WTD [47–64], which quantifies the probability of observing electron transfer events at different time intervals. The WTDs have been extensively used to analyze electron transport in QDs [47–51, 63, 65, 66], revealing coherent oscillations [47, 63], entanglement signatures [63], identifying the Majorana states for the Majorana island device [65], and the influence of non-Markovian environments [51].

Despite advances in understanding non-Markovian transport, its interplay with the Kondo effect in shaping the WTD remains largely unexplored. This work aims to bridge this gap by studying a single impurity Anderson model (SIAM), describing a QD ultra-strongly coupled to a (left) non-Markovian lead and weakly coupled to a detector (right) Markovian lead. This allows us to combine the HEOM, describing the interaction with the left lead, with a master equation to describe the right detector lead and allow us to obtain the WTD.

This approach reveals the emergence of short-time oscillations in the WTD. These oscillations become more pronounced when increasing the left-lead coupling. Fourier analysis reveals this stronger coupling induces a blue shift in the frequency domain, signifying the enhanced system-environment interactions. Crucially, these oscillations are absent when using the dressed master equation alone, confirming their non-Markovian origin.

Furthermore, we explore the Kondo resonance's influence on the WTD. Increasing Coulomb interactions within the dot (impurity) strengthens the Kondo reso-

* These authors contributed equally to this work.

† nwlambert@gmail.com

‡ cirio.mauro@gmail.com

§ yuehnan@mail.ncku.edu.tw

nance in the density of states (DOS), as expected. Correspondingly, the WTD oscillations are amplified, demonstrating an indirect link between the Kondo effect and non-Markovian transport dynamics.

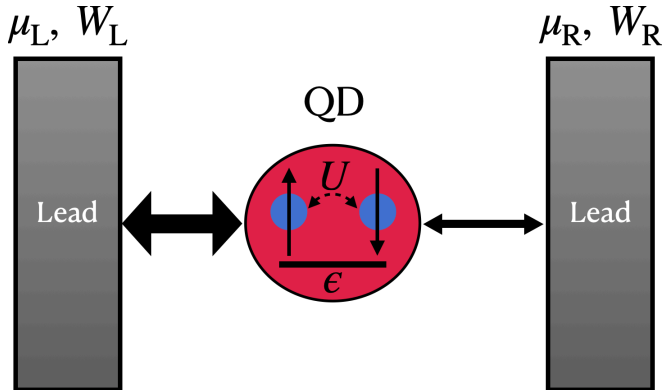


FIG. 1. Schematic representation of the SIAM considered in this study. The model depicts a single quantum dot (QD) with spin configurations, ultrastrongly coupled to a left bath (L) and weakly coupled to a right bath (R). The energy of the electronic state in the QD is denoted by ϵ . U represents the Coulomb repulsion energy between two electrons with opposite spins occupying the QD. Here, W_α and μ_α represent the bandwidth and chemical potential of the lead ($\alpha = \text{L, R}$), respectively.

II. MODEL

We consider a SIAM as depicted in Fig. 1. The system is comprised of a QD (the single impurity) coupled to two leads. The QD can be occupied by either a single electron or two electrons with different spin configurations $\sigma = \uparrow, \downarrow$ (up, down). The total Hamiltonian of the system and leads is ($\hbar = 1$)

$$H_T = H_s + H_f + H_{\text{sf}}. \quad (1)$$

Here, the impurity is described by the system Hamiltonian

$$H_s = \sum_{\alpha=\uparrow,\downarrow} \epsilon \hat{n}_\sigma + U \hat{n}_\uparrow \hat{n}_\downarrow, \quad (2)$$

where the operator $\hat{n}_\sigma = d_\sigma^\dagger d_\sigma$ describes the number of electrons with spin σ in the QD, each associated with the annihilation operator d_σ and the energy-level scale ϵ . The Coulomb interaction between two electrons has a strength given by the repulsion energy U and is described by the non-linear operator $\hat{n}_\uparrow \hat{n}_\downarrow$.

The leads are described by the Hamiltonian

$$H_f = \sum_{k,\alpha,\sigma} \omega_{k,\alpha,\sigma} c_{k,\alpha,\sigma}^\dagger c_{k,\alpha,\sigma}, \quad (3)$$

where $c_{k,\alpha,\sigma}$ creates an electron in the state k of the α -th lead ($\alpha \in \{\text{L, R}\}$). The tunneling between the QD and

the leads is given by

$$H_{\text{sf}} = \sum_{k,\alpha,\sigma} g_{k,\alpha,\sigma} \left(c_{k,\alpha,\sigma}^\dagger d_\sigma + c_{k,\alpha,\sigma} d_\sigma^\dagger \right), \quad (4)$$

parametrized by the coupling strengths $g_{k,\alpha,\sigma}$. In the continuum limit, these coefficients can be encoded in a spectral density function for which we choose a Lorentzian lineshape

$$J_\alpha(\omega) = \frac{1}{2\pi} \frac{\Gamma_\alpha W_\alpha^2}{(\omega - \mu_\alpha)^2 + W_\alpha^2}. \quad (5)$$

Here, Γ_α describes the overall coupling strength between the QD and the α -lead, while W_α and μ_α represent the bandwidth and the chemical potential of the α -lead, respectively.

In this work, we assume the system to be ultra-strongly coupled to the left lead and only weakly coupled to the right one, which can thereby be used as a detector with a well-defined WTD. The effects of the fermionic leads on the system are fully encoded in the two-time correlation functions

$$\begin{aligned} C_\alpha^\nu(t) &= \text{Tr}_f \left[\sum_k \Gamma_{\alpha,k}^2 d_\sigma^\nu d_{\bar{\sigma}}^\nu \rho_f(0) \right] e^{\nu i \omega t} \\ &= \frac{1}{2\pi} \int_{-\infty}^{\infty} d\omega J_\alpha(\omega) \left[\frac{1-\nu}{2} + \nu n_\alpha^{\text{eq}}(\omega) \right] e^{\nu i \omega t}, \end{aligned} \quad (6)$$

in terms of the Fermi-Dirac distribution $n_\alpha^{\text{eq}}(\omega) = \{\exp[(\omega - \mu_\alpha)/k_B T] + 1\}^{-1}$ at temperature T , where k_B is the Boltzmann constant. Here $\nu = \pm 1$ characterizes the distinction between particles and holes, and $d_\sigma^{\nu=1} = d_\sigma^\dagger$ and $d_\sigma^{\nu=-1} = d_\sigma$ (with $\bar{\nu} = -\nu$). While the correlations in Eq. (6) cannot in general be written in a closed analytical form, it is usually advantageous to consider the following ansatz

$$C_\alpha^\nu(t) = \sum_{l=0}^{l_{\text{max}}} \eta_l^\nu \exp[-\gamma_{\alpha,\nu,l}(t)]. \quad (7)$$

This representation expresses the correlation as an exponential series whose strength-coefficients η_l^ν and decay rates $\gamma_{\alpha,\nu,l}$ can be found using the Padé spectral decompositions as in [67, 68].

In order to capture the non-perturbative effects originating from the strong interaction with the left lead, we employ the HEOM approach [68–70] which is, in principle, numerically exact [71] as it goes beyond the standard master equations based on the Born-Markov approximation.

This enables us to comprehensively explore the interplay between system-bath correlations and non-Markovian transport characteristics. Explicitly, the

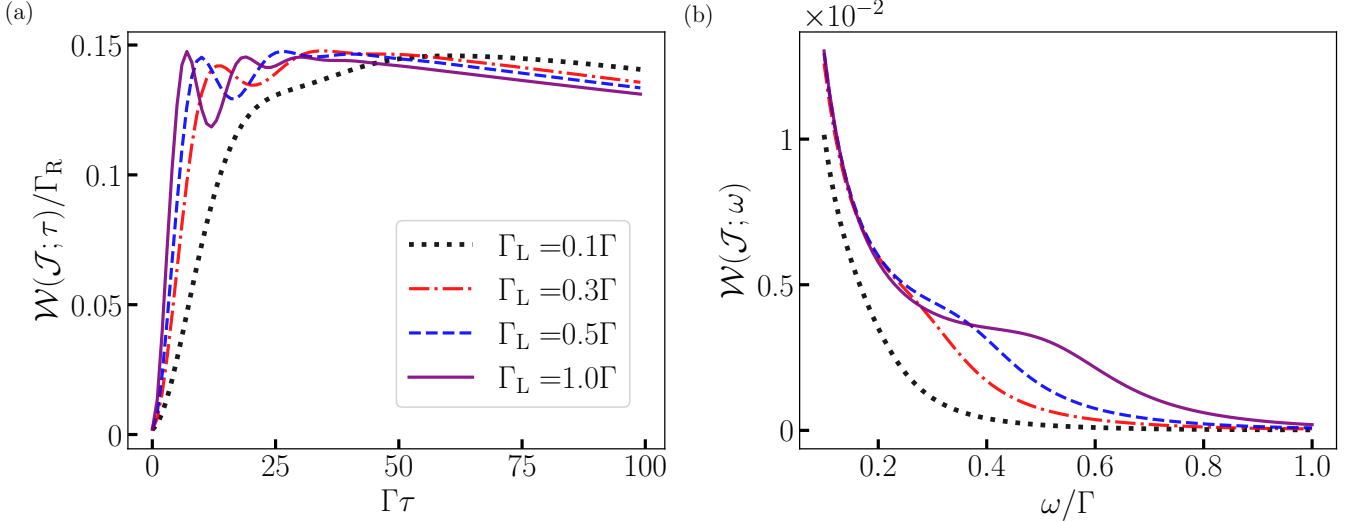


FIG. 2. (a) $\mathcal{W}(\mathcal{J}; \tau)/\Gamma_R$ as a function of time Γt for different values of Γ_L with $U = 1\Gamma$, where $\Gamma_R = 0.01\Gamma$. The WTD exhibits oscillations that become more pronounced as Γ_L increases. (b) Spectrum of the WTD, $\mathcal{W}(\mathcal{J}; \omega)$, obtained via the Fourier transform of $\mathcal{W}(\mathcal{J}; \tau)$ (Eq. (23)). As Γ_L increases, the WTD spectrum shows not only an increase in the oscillation amplitude but also a blue shift in the oscillation frequency.

HEOM for the strongly coupled QD-(left lead) system can be written as

$$\partial_t \rho_{\mathbf{j}}^{(m,p)}(t) \equiv \hat{\mathcal{M}} \rho_{\mathbf{j}}^{(m,p)}(t), \quad (8)$$

in terms of the HEOM Liouvillian superoperator $\hat{\mathcal{M}}$, which characterizes the dynamics of the set of auxiliary density operators (ADOs) defined by $\rho_{\mathbf{j}}^{(m,p)}(t)$. Here, the pair (m, p) represents the m th level fermionic ADO with parity p , and \mathbf{j} denotes the vector $[j_m, \dots, j_1]$, where each j represents a specific ensemble with multi-index $\{\alpha, v, h, \sigma_f\}$ in which σ_f specifies the remaining system quantum numbers. The superoperator in Eq. (8) can be explicitly defined by its action on the auxiliary density matrices as

$$\begin{aligned} \hat{\mathcal{M}} \rho_{\mathbf{j}}^{(m,p)}(t) = & - \left(i \hat{\mathcal{L}}_s + \sum_{w=1}^m \gamma_{q_w} \right) \rho_{\mathbf{j}}^{(m,p)}(t) \\ & - i \sum_{\substack{j' \notin \mathbf{j} \\ m}} \hat{\mathcal{A}}_{j'} \rho_{\mathbf{j}+}^{(m+1,p)}(t) \\ & - i \sum_{w=1}^m (-1)^{m-w} \hat{\mathcal{B}}_{q_w} \rho_{\mathbf{j}-}^{(m-1,p)}(t). \end{aligned} \quad (9)$$

Here, $\hat{\mathcal{L}}_s[\cdot] = [H_s(t), \cdot]$ describes the system dynamics while $\hat{\mathcal{A}}_j$ and $\hat{\mathcal{B}}_j$ are the fermionic superoperators describing the system-bath interaction. Specifically, they couple the m th-level-fermionic ADOs to the $(m+1)$ th-level- and $(m-1)$ th-level-fermionic ADOs and they are explicitly given by

$$\begin{aligned} \hat{\mathcal{A}}_j[\cdot] &= (-1)^{\delta_{p,-}} \{ d_{\sigma_f}^{\nu}[\cdot] - \hat{\mathcal{P}}_s [[\cdot] d_{\sigma_f}^{\bar{\nu}}] \}, \\ \hat{\mathcal{B}}_j[\cdot] &= (-1)^{\delta_{p,-}} \{ \eta_{\alpha,h}^{\nu} d_{\sigma_f}^{\nu}[\cdot] + (\eta_{\alpha,h}^{\bar{\nu}})^* \hat{\mathcal{P}}_s [[\cdot] d_{\sigma_f}^{\nu}] \}, \end{aligned} \quad (10)$$

in terms of the parity operator $\hat{\mathcal{P}}_s$ whose action is defined as

$$\hat{\mathcal{P}}_s \left[\rho_{\mathbf{j}}^{(m,\pm)}(t) d_{\sigma_f}^{\nu} \right] = \mp (-1)^m \rho_{\mathbf{j}}^{(m,\pm)}(t) d_{\sigma_f}^{\nu}. \quad (11)$$

In contrast, the coupling to the right lead (which will

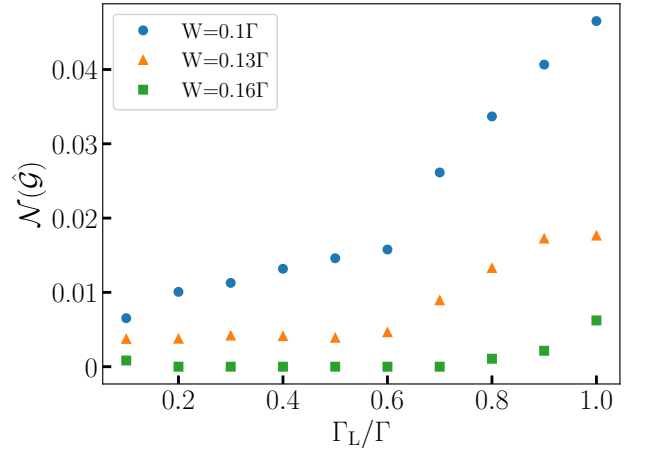


FIG. 3. Non-Markovianity ($\mathcal{N}(\hat{\mathcal{G}})$) as a function of the coupling strength between the quantum dot (QD) and the left lead (Γ_L) for different values of the environment's bandwidth (W). The truncation of the HEOM tiers and the Padé series are set to $N_H = 4$ and $l_{\max} = 2$, respectively. The results show that the non-Markovianity becomes less significant as W increases. This trend is observed for all values of Γ_L presented. In other words, at a smaller fixed bandwidth (e.g., $W = 0.1\Gamma$), a stronger Γ_L leads to an even higher degree of $\mathcal{N}(\hat{\mathcal{G}})$.

primarily serve as a detector) can be modeled using the typical assumptions valid in the weak-coupling regime. This allows for an adequate description of the right-lead influence on the QD using the Born-Markov quantum master equation. At the same time, when strong system interactions are present, such as those arising from a large Coulomb repulsion U in the QD, the conventional local Lindblad master equation can become unreliable. This unreliability can manifest in unphysical predictions, including excitations at absolute zero temperature [72] or inaccurate electron occupation numbers within the QD. To overcome these problems, it is possible to use a dressed Born-Markov master equation (dBMMME) which is more accurate than the conventional local Lindblad master equation [32] to model these regimes. This improvement relies on restricting bath-induced transitions among system eigenstates $|\varphi_i\rangle$ of H_s having energy ϵ_i . Technically, this corresponds to writing the Lindblad dissipator using the eigenbasis decomposition

$$\begin{aligned} \partial_t \rho_s(t) = & -i[H_s, \rho_s(t)] + \sum_{\alpha, \sigma} \sum_{\epsilon_k - \epsilon_l = \omega} \sum_{p=\pm} \gamma_{\alpha, l \rightarrow k}(\omega) \times \\ & \left\{ p |\varphi_k\rangle \langle \varphi_l| \rho_s^p(t) \langle \varphi_l| \langle \varphi_k| - \frac{1}{2} \{ |\varphi_l\rangle \langle \varphi_l|, \rho_s^p(t) \} \right\}, \end{aligned} \quad (12)$$

where $[\cdot, \cdot]$ and $\{\cdot, \cdot\}$ denote the commutator and anti-commutator, respectively. The transition rates in this dBMMME equation are explicitly given by

$$\gamma_{\alpha, l \rightarrow k}(\omega) = 2\pi \sum_{\nu=\pm 1} \sum_{\sigma=\uparrow, \downarrow} |\langle \varphi_k | d_{\sigma}^{\nu} | \varphi_l \rangle|^2 J_{\alpha}(\omega) n_{\alpha}^{\text{eq}}(\omega). \quad (13)$$

The full equation of motion can be obtained by incorporating the strong coupling effects [described by Eq. (8)] and the weak coupling effects [described by Eq. (12)] to model both non-Markovian and weak interaction to the left and right leads, respectively. This is achieved by replacing the $\hat{\mathcal{L}}_s[\cdot]$ term in Eq. (9) with the right-hand side of Eq. (12). Of course, this approximation for the right lead neglects hybridization between the system and the left lead, but we have found (compared to a full HEOM simulation by calculating the electron occupation number for both leads) that these effects are negligible.

In order to analyze the statistical properties of the electron transport phenomena, WTD plays a crucial role. In fact, electronic currents are defined by a series of individual electron tunneling events occurring at random time intervals. The WTD quantifies the probability of observing an electron transfer in the detector electrode at a specific time $t + \tau$, given that an electron was previously detected in the same electrode at an earlier time t . Given its experimental accessibility and also for analytical convenience, we now compute the WTD around the steady state of this model we have described. The WTD in the steady state is derived as follows [47, 55–57, 63, 65]

$$\mathcal{W}(\mathcal{J}; \tau) = \frac{\text{Tr} \left[\mathcal{J} e^{\hat{\mathcal{M}}_0 \tau} \mathcal{J} \rho_{\text{st}} \right]}{\text{Tr} \left[\mathcal{J} \rho_{\text{st}} \right]}. \quad (14)$$

In this equation, ρ_{st} is the steady state of the auxiliary density operator (ADO) space, \mathcal{J} is a superoperator encoding the quantum jumps in the dynamics, and $\hat{\mathcal{M}}_0 = \hat{\mathcal{M}} - \mathcal{J}$ is the superoperator evolving the system in the absence of quantum jumps. Assuming conditions in which the right lead only acts as a sink for electrons, using Eq. (12), the quantum jump operator reads

$$\begin{aligned} \mathcal{J}[\rho_s] &= \sum_{\epsilon_k - \epsilon_l = \omega} \gamma_{\alpha, l \rightarrow k}(\omega) |\varphi_k\rangle \langle \varphi_l| \rho_s(t) |\varphi_l\rangle \langle \varphi_k| \\ &\equiv \sum_{i=1}^4 \mathcal{J}_i[\rho_s], \end{aligned} \quad (15)$$

where the definition in the last line is introduced to highlight specific electron transfer processes from the QD to the right lead. Explicitly,

$$\begin{aligned} \mathcal{J}_1[\rho_s] &= \gamma_{\text{R}, \uparrow \rightarrow 0}(-\epsilon) |0\rangle \langle \uparrow | \rho_s | \uparrow \rangle \langle 0| \\ \mathcal{J}_2[\rho_s] &= \gamma_{\text{R}, \downarrow \rightarrow 0}(-\epsilon) |0\rangle \langle \downarrow | \rho_s | \downarrow \rangle \langle 0| \\ \mathcal{J}_3[\rho_s] &= \gamma_{\text{R}, \uparrow \downarrow \rightarrow \downarrow}(-U) | \downarrow \rangle \langle \uparrow \downarrow | \rho_s | \uparrow \downarrow \rangle \langle \downarrow | \\ \mathcal{J}_4[\rho_s] &= \gamma_{\text{R}, \uparrow \downarrow \rightarrow \uparrow}(-U) | \uparrow \rangle \langle \uparrow \downarrow | \rho_s | \uparrow \downarrow \rangle \langle \uparrow |, \end{aligned} \quad (16)$$

so that \mathcal{J}_i describes transitions from the single-occupancy states $|\sigma\rangle$ ($\sigma = \uparrow, \downarrow$) to the vacuum $|0\rangle$ for $i = 1, 2$, and from the double-occupancy state $|\uparrow \downarrow\rangle$ to one with single-occupancy for $i = 3, 4$.

We can also define WTD for a specific electron transfer process, described by the quantum jump superoperator \mathcal{J}_i , with

$$w_i(\tau) \equiv \mathcal{W}(\mathcal{J}_i; \tau) = \frac{\text{Tr} \left[\mathcal{J}_i e^{\hat{\mathcal{M}}_0^i \tau} \mathcal{J}_i \rho_{\text{st}} \right]}{\text{Tr} \left[\mathcal{J}_i \rho_{\text{st}} \right]}, \quad (17)$$

where $\hat{\mathcal{M}}_0^i = \hat{\mathcal{M}} - \mathcal{J}_i$ represents the superoperator governing the evolution without the specific jump process \mathcal{J}_i .

Since the left lead is allowed to exhibit non-Markovian effects, it is useful to introduce a measure to quantify the degree of non-Markovianity. In a Markovian process, information flows unidirectionally from the system to the environment, leading to increasingly indistinguishable quantum states over time. Conversely, non-Markovian behavior allows for information to flow back to the system, potentially overcoming this loss of distinguishability. The trace distance, defined as

$$D(\rho_1, \rho_2) = \frac{1}{2} \text{Tr} \left[\sqrt{(\rho_1 - \rho_2)^\dagger (\rho_1 - \rho_2)} \right], \quad (18)$$

quantifies the distinguishability between two quantum states, ρ_1 and ρ_2 . From Eq. (8), the reduced state of the QD system is defined as

$$\rho_s(t) = \rho^{(0,+)}(t) = \hat{\mathcal{G}}(t) [\rho^{(0,+)}(0)], \quad (19)$$

where $\hat{\mathcal{G}}(t) = \exp(\hat{\mathcal{M}}t)$ is the superoperator which propagates all ADOs. For a Markovian process, the distinguishability $D(\rho_{s1}(t), \rho_{s2}(t))$ between two different initial states $s1$ and $s2$ of the QD monotonically decreases

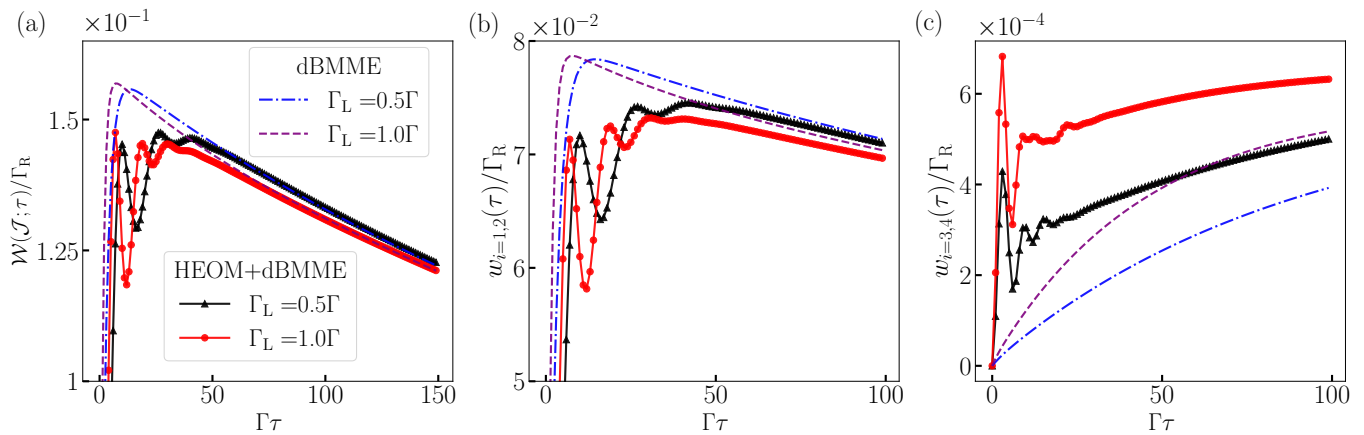


FIG. 4. (a) $\mathcal{W}(\mathcal{J}; \tau)$ calculated by using HEOM+dBMME method (solid) and dBMME (dashed). In the strong coupling regime ($\Gamma_L > \dots$), dBMME fails to capture short-time oscillations. (b), (c) Individual electron WTDs, $w_i(\tau)$, at $\Gamma_L = 0.5\Gamma$ and $\Gamma_L = \Gamma$. HEOM+dBMME reveals significant short-time oscillations in all $w_i(\tau)$ – a feature absent in dBMME results. Electrons predominantly emit from single occupation states ($|\uparrow\rangle$ or $|\downarrow\rangle$, related to $\mathcal{J}_{1,2}$) rather than the double occupation state ($|\uparrow\downarrow\rangle$, $\mathcal{J}_{3,4}$)

over time. However, for non-Markovian systems, a non-monotonic behavior emerges as a result of information backflow. As a consequence, we can quantify the degree of non-Markovianity by considering the difference in distinguishability with respect to the Markovian case for all possible initial states as

$$\mathcal{N}(\hat{\mathcal{G}}) = \max_{\rho_{s1}, \rho_{s2}(0)} \sum_i [D(\rho_{s1}(b_i), \rho_{s2}(b_i)) - D(\rho_{s1}(a_i), \rho_{s2}(a_i))]. \quad (20)$$

Here the index i labels the times intervals (a_i, b_i) during which the rate of change of the trace distance is positive, indicating an increase in distinguishability due to non-Markovian information flow [12], i.e.,

$$\frac{d}{dt} D(\rho_{s1}(t), \rho_{s2}(t)) > 0, \quad (21)$$

for $t \in (a_i, b_i)$. In the following section, we use these technical tools to analyze the electronic transport properties of the model defined in Eq. (1).

III. RESULTS

We begin with an analysis of the full WTD for different values of the coupling strength to the bath Γ_L with a constant on-site Coulomb interaction energy of $U = 1\Gamma$, and for a system initially at equilibrium with chemical potential $\mu = 0$. Here and throughout the article, we use Γ as a reference scale for all energy parameters. In Fig. 2 we show the short-time behavior of the WTD, where we further set $k_B T = 0.5\Gamma$, and constrained the energy of the QD level to $\epsilon = -0.1\Gamma$

A. WTD reveals non-Markovian signature

To compute the distinguishability of the states during the dynamics, we used Eq. (20) by maximizing over all pairs of initial conditions taken from the set $\{|0\rangle, |\uparrow\rangle, |\downarrow\rangle, |\uparrow\downarrow\rangle, |+\rangle, |-\rangle\}$ where $|\pm\rangle = 1/\sqrt{2}(|\uparrow\rangle \pm |\downarrow\rangle)$. As expected, non-Markovian effects become increasingly pronounced as the system transitions into the non-Markovian regime. This observation is evident in Fig. 3, where stronger coupling strengths (Γ_L ranging from 0.1Γ to Γ) lead to an increase in distinguishability. We observe that this feature is absent when the HEOM is replaced with a Markovian master equation to model the strong coupling to the left lead, demonstrating its inability to capture non-Markovian effects. On the other hand, the result using the HEOM further shows that this effect is particularly pronounced when the lead bandwidths ($W_{L,R} = W$) are narrower, specifically for $W < 0.16\Gamma$. This suggests that narrower fermionic bandwidths can amplify non-Markovian effects.

To analyze the influence of the system-bath coupling strength on non-Markovianity, we now investigate the waiting-time distribution (WTD), $\mathcal{W}(\mathcal{J}; \tau)$, across different values of Γ_L at constant bandwidth $W_{L,R} = W = 0.1\Gamma$ for the leads. As shown in Fig. 2(a), a key feature emerges in the behavior of $\mathcal{W}(\mathcal{J}; \tau)$. In fact, in a regime where $\Gamma_L > 0.1\Gamma$, oscillations in the waiting time distribution emerge. Interestingly, the frequency of these oscillations increases for stronger interactions between the system and the left lead. We remark that, here, this behavior is driven by system-bath interactions rather than the presence of coherent interactions [73, 74], or spin-state transitions within the system [53, 75].

To further describe the oscillatory behavior of the

WTD, we now consider its one-sided Fourier transform

$$\mathcal{W}(\mathcal{J}; \omega) = \left| \int_0^\infty d\tau e^{i\omega\tau} \mathcal{W}(\mathcal{J}; \tau) \right|, \quad (22)$$

which can be written as [63]

$$\mathcal{W}(\mathcal{J}; \omega) = \left| \frac{\text{Tr} \left[\mathcal{J} \left(i\omega \mathbb{1} - \hat{\mathcal{M}}_0 \right)^{-1} \mathcal{J} \rho_{\text{st}} \right]}{\text{Tr} [\mathcal{J} \rho_{\text{st}}]} \right|. \quad (23)$$

We analyze this quantity in Fig. 2(b) where we observe an overall shift in the oscillation frequencies as Γ_L increases. This justifies the origin of this shift with the emergence of a stronger system-bath hybridization. We note that an equivalent behavior is also present using a simplified model in which the impurity is replaced by a single charge (see Appendix A for details).

To confirm the role of the non-perturbative effects in capturing the WTD oscillations, in Fig. 4, we compare the results when either the HEOM or the dBMME is used to describe the strong interaction to the left lead. As expected, the dBMME approach is not able to correctly model the non-perturbative effects characterizing the coupling to the left lead, thereby failing to reproduce the WTD oscillations shown by the HEOM.

In order to refine this analysis to find the dominant processes in the electronic transport, we now calculate the individual waiting time distributions $w_i(\tau)$ for each quantum jump defined in Eq. (15). These are the WTD for electrons tunneling out of the QD from its single-occupancy states ($|\sigma = \uparrow, \downarrow\rangle$, for $i = 1, 2$) and the double-occupancy state ($|\uparrow\downarrow\rangle$, for $i = 3, 4$).

In Fig. 4(b) and (c), we observe that the peak probability of $w_{i=1,2}(\tau)$ is significantly higher than that of $w_{i=3,4}(\tau)$. This indicates a preference for the QD to occupy single-occupancy states, likely due to the large on-site Coulomb repulsion energy (U) disfavoring double occupancy. In other words, tunneling to the right lead is dominated by events involving the QD single occupancy states. However, the presence of oscillatory behavior for all $w_i(\tau)$ suggests that events involving single-to-empty and double-to-single state transitions are both influenced by the coherent effects characterizing the interaction to the left lead. In addition to the identical jump events in the WTD, we also investigated components of $\mathcal{W}(\mathcal{J}; \tau)$ incorporating two distinct quantum jump events. These components exhibited only minor contributions to $\mathcal{W}(\mathcal{J}; \tau)$, implying weak correlations between different jump types. The detail is presented in Appendix B. It is interesting to further analyze the relation between these non-Markovian features and the emergence of entanglement between the QD and the bath electrons which leads to the Kondo effect.

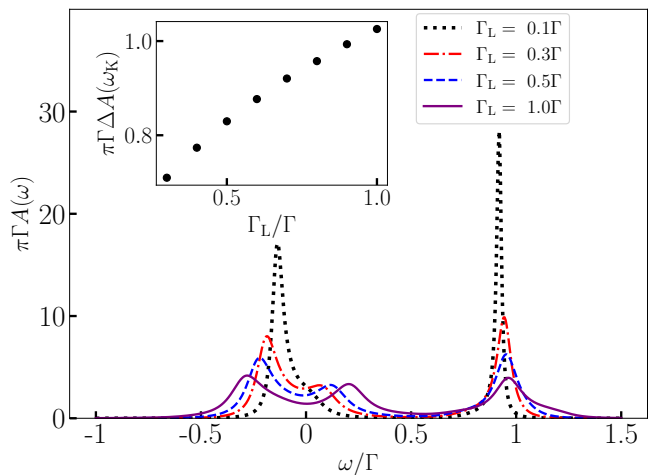


FIG. 5. Density of states and Kondo resonance dependence on coupling strength. $A(\omega)$ is the Spin-up electron density of states $A(\omega)$. Two Hubbard peaks appear, along with a central Kondo peak for $\Gamma_L \geq 0.3\Gamma$. The Kondo peak signifies an equilibrium many-body entangled state between the QD and left lead, and its intensity increases slightly with coupling strength (inset). Inset: $\Delta A(\omega_K)$, the difference in Kondo peak intensity between $k_B T = 0.5\Gamma$ and $k_B T = 5\Gamma$, as a measure of Kondo resonance. Larger $\Delta A(\omega_K)$ correlates with stronger coupling and higher-frequency oscillations in $\mathcal{W}(\mathcal{J}; \tau)$

B. WTD and the Kondo correlation

To analyze the interplay between non-Markovianity and Kondo physics, we introduce the DOS of the QD, which is an important quantity to characterize the electronic behavior of the system [76]. The DOS of the QD

$$\pi A_\sigma(\omega) = \text{Re} \left\{ \int_0^\infty dt \langle \{d_\sigma(t), d_\sigma^\dagger(0)\} \rangle e^{i\omega t} \right\}, \quad (24)$$

depends on system correlations which can be computed using the parity-dependent HEOM approach [68, 77] in Eq. (8) and Eq. (12). Here, $\langle \hat{O} \rangle$ denotes the expectation value of the system operator \hat{O} . In the absence of an applied magnetic field, the QD exhibits spin-independent DOS. Therefore, in the following, we will focus on the DOS of the spin-up state, i.e., on the quantity $A(\omega) \equiv A_{\sigma=\uparrow}(\omega)$. As shown in Fig. 5, the DOS exhibits two Hubbard peaks located, for weak system-bath coupling, at the resonant energies ϵ and $\epsilon + U$ corresponding to singly and double occupied states, respectively. At strong coupling to the left lead, a central Kondo resonance peak appears as a manifestation of the equilibrium many-body entanglement between single electron states in the system and the electrons in the reservoir continuum.

Increasing Γ_L slightly enhances and blue-shifts the Kondo peak. However, this increase is subtle due to the proximity of the single-occupation distribution to the Kondo resonance. This proximity can be attributed to the central peak height. Since Kondo correlations are

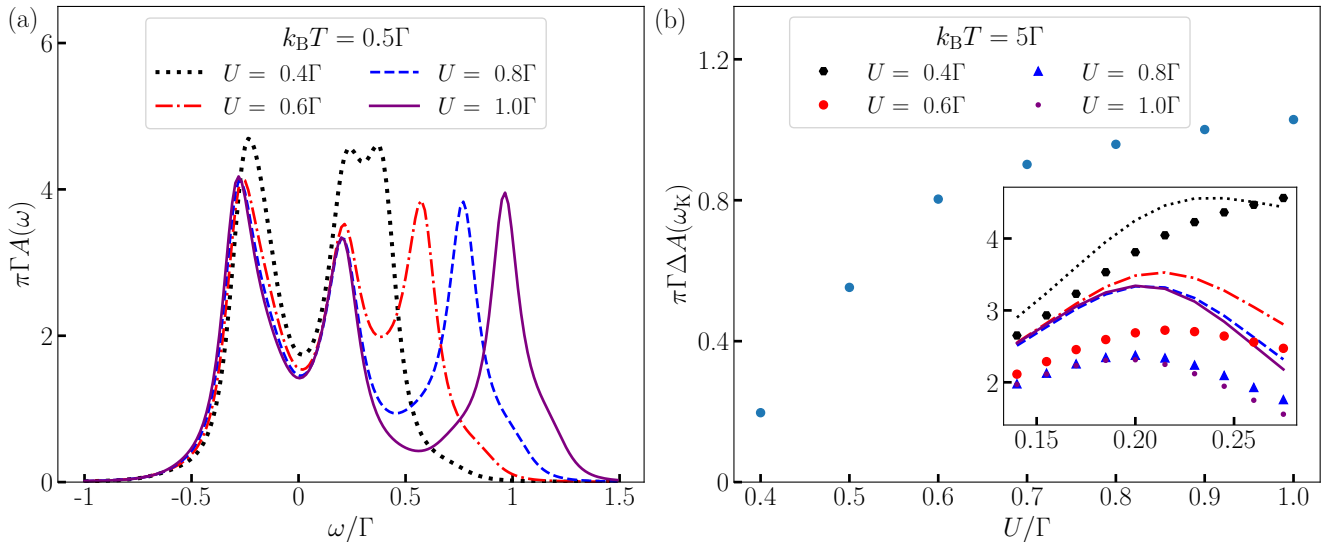


FIG. 6. (a) Density of states (DOS) for varying Coulomb repulsion energies, U . (b) Difference in Kondo peak intensity between $k_B T_1 = 0.5\Gamma$ and $k_B T_2 = 5\Gamma$, a measure of Kondo resonance strength. Larger differences correspond to stronger Kondo resonance at larger U . Inset: Kondo peaks at both temperatures (curves: $k_B T = 0.5\Gamma$; scatters: $k_B T = 5\Gamma$).

highly temperature-sensitive (thermal fluctuations readily disrupt them [25, 78–80]), increasing the lead temperature rapidly suppresses the DOS Kondo peak [32, 81–83].

To isolate the true Kondo correlation within the DOS, we examine how the Kondo peak diminishes as the temperature exceeds the Kondo temperature (where the DOS central peak height remains fixed). We compare a higher temperature, $T_2 = 5\Gamma$, to a lower one, $T_1 = 0.5\Gamma$, and calculate the difference in Kondo peak height:

$$\Delta A(\omega_K) = A(\omega_K, T_1) - A(\omega_K, T_2), \quad (25)$$

where ω_K is the Kondo peak frequency. As Γ_L increases, $\Delta A(\omega_K)$ also increases, signifying a stronger Kondo correlation induced by the enhanced QD-lead coupling (see the inset in Fig. 5).

In this specific instance, one can quantify the strength of the Kondo correlation from the properties of the DOS. However, in cases when the dependence of the Kondo-peak height with respect to the lead-coupling is difficult to resolve, oscillations in the WTD could serve as an alternative indicator to quantify the effects of system-bath non-Markovianity on the Kondo correlation.

Intriguingly, when the SIAM’s repulsion energy U is significantly reduced, its WTD behavior exhibits similarities to that of the coupled charge-lead system. This observation highlights the crucial role of the repulsion energy in differentiating the SIAM’s behavior from the charge-lead system. Moreover, the repulsion energy U contributes to the formation of a localized magnetic moment at the QD site by energetically penalizing the occupation of the same site with a second electron. This

localized moment then interacts with the conduction electrons in the lead, giving rise to the Kondo correlations. As we increase U from 0.4Γ to Γ within the SIAM system, we observe not only the expected blue shift of the positive frequency Hubbard peak, but also a reduction in the central peak’s height [Fig. 6(a)]. Importantly, this decrease in the central peak is primarily due to the diminished contribution of double-occupancy distribution. The positive-frequency Hubbard peak significantly overlaps the central peak at smaller U values. Consequently, it becomes challenging to quantify the Kondo peak solely through DOS analysis. However, as shown in Fig. 6(b), $\Delta A(\omega_K)$ increases at larger U values. This trend indicates stronger Kondo resonances in the presence of a more intense Coulomb repulsion energy. This is illustrated in the inset of Fig. 6(b) which compares the DOS around the Kondo peak frequency at two temperatures, T_1 and T_2 . At the higher temperature ($T_2 = 5\Gamma$), the Kondo peak is suppressed. Consequently, the difference $\Delta A(\omega_K)$ directly reflects this change in the Kondo resonance’s strength.

To gain more insight, we examine the influence of U on the WTD. By defining $w_i(\omega)$ as the Fourier-transform of $w_i(\tau)$, we observe that an increase in U causes an amplification of the oscillation width for $w_{i=1}(\omega)$ and a suppression for $w_{i=3}(\omega)$, see Fig. 7(a) and Fig. 7(c), respectively. This is due to the fact a strong Coulomb blockade reduces the probability of double occupancy, thereby increasing the frequency of jump events from $|\sigma\rangle$ (for $\sigma = \uparrow$ or \downarrow) to the empty state.

Since a larger U effectively increases the separation between the QD singly and doubly occupied states, it also increases the stability of the localized magnetic moment,

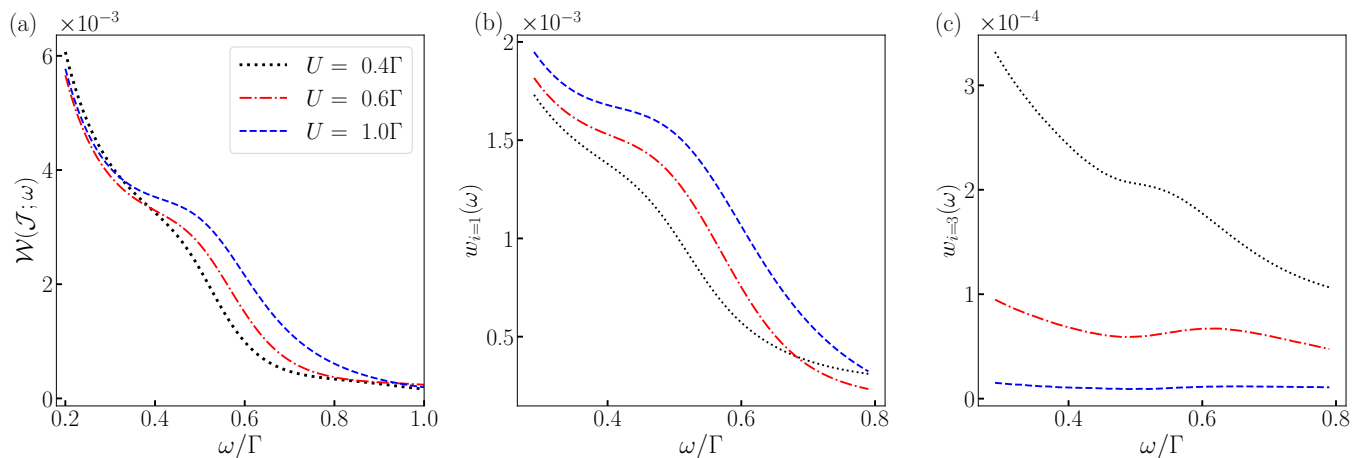


FIG. 7. Fourier-transformed WTD for different U . (a) $\mathcal{W}(\mathcal{J}; \omega)$. The oscillation amplitude increases with stronger Coulomb interaction U . (b), (c) Individual Fourier-transformed WTDs $w_{i=1}(\omega)$ and $w_{i=3}(\omega)$, showing enhanced oscillations for $w_{i=1}(\tau)$ and suppressed oscillations for $w_{i=3}(\tau)$ with increasing U .

thereby enhancing the Kondo correlations by making the system more conducive to Kondo screening. As a consequence, this demonstrates that a larger oscillation amplitude for the quantities $\mathcal{W}(\mathcal{J}; \omega)$ and $w_{i=1}(\omega)$ coincide with, and can serve as an indicator of, an enhancement of the Kondo resonance.

IV. CONCLUSIONS

In summary, we have investigated the non-Markovian transport dynamics in a single impurity Anderson model. Specifically, we considered a quantum dot ultrastrongly coupled to a lead injecting electrons and weakly coupled to a detector-lead. At short times, we observed the emergence of non-Markovianity signatures in terms of oscillations in the waiting time distribution (evaluated numerically using the hierarchical equations of motion and a Born-Markov master equation).

As the coupling to the injecting lead is increased, these oscillations become more pronounced and blue-shifted in frequency. This effect is due to the hybridization between the system and the ultra-strongly coupled lead as confirmed by the impossibility to reproduce it using a Markovian master equation.

By tuning the Coulomb repulsion in the quantum dot, we further explored the corresponding signatures in terms of the Kondo effect. In fact, by increasing the interaction between electrons in the dots, we observed the concurrent enhancement of both the Kondo resonance and the oscillations in the waiting time distribution. This sheds light on the relations and influence between non-Markovian system-bath correlations and the properties of the electron waiting time distribution and Kondo physics. As an outlook, this work could be extended by calculating the WTD deep in the Kondo regime using fermionic pseudomodes to model strong system-bath interactions [84].

At the same time, an analysis of the full counting statistics [16, 59, 66, 85] using the hierarchical equations of motion could further illuminate the role of non-Markovian effects in electron transport.

V. ACKNOWLEDGEMENT

YNC acknowledges the support of the National Center for Theoretical Sciences and the National Science and Technology Council, Taiwan (NSTC Grants No. 112-2123-M-006-001). M.C. acknowledges support from NSFC (Grant No. 11935012) and NSAF (Grant No. U2330401). N. L. is supported by the RIKEN Incentive Research Program and by MEXT KAKENHI Grant Numbers JP24H00816, JP24H00820.

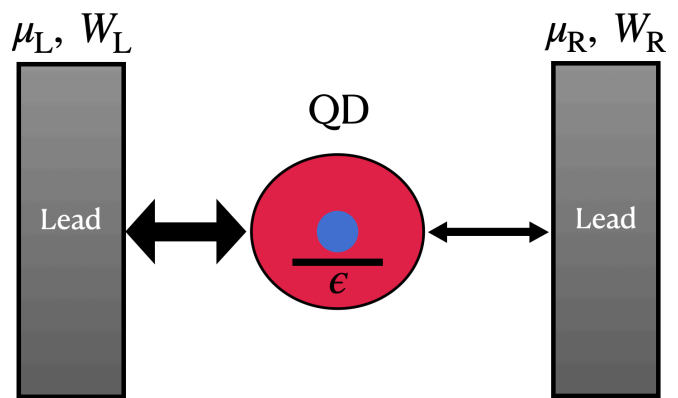


FIG. 8. A quantum dot (QD) with a single energy level (ϵ) is ultra-strongly coupled to its left lead (characterized by a bandwidth $W_L = 0.1\Gamma$ and a chemical potential $\mu_L = 0$) and weakly coupled to its right lead (characterized by $W_R = 0.1\Gamma$ and $\mu_R = 0$). A detector placed in correspondence to the right lead is assumed to measure the waiting time distribution $\mathcal{W}(\mathcal{J}; \tau)$.

Appendix A: single charge

To gain more intuition over the physics analyzed in the main text, here we consider a system made out of a single charge, see Fig. 8. By comparing the results of the HEOM and a Markovian master equation, we show that, even in this simplified setting, non-Markovian effects cause the emergence of oscillations in the WTD. We further characterize the blue shift on the oscillation frequency using a pseudo-fermion toy-model.

1. Model

We consider a single charge coupled to two leads, as shown in Fig. 8 and described by the Hamiltonian

$$\begin{aligned}
 H_s &= \epsilon d^\dagger d, \\
 H_f &= \sum_{k,\alpha} \omega_{k,\alpha} c_{k,\alpha}^\dagger c_{k,\alpha} \\
 H_{sf} &= \sum_{k,\alpha} g_{k,\alpha} c_{k,\alpha}^\dagger d + g_{k,\alpha}^* d^\dagger c_{k,\alpha}.
 \end{aligned} \tag{A1}$$

Here, d^\dagger creates an electron in the QD, while $c_{k,\alpha}^\dagger$ creates an electron in the lead $\alpha \in \{L,R\}$. In the absence of Coulomb interactions within the QD, the quantum jump superoperator for this single charge case simplifies to $\mathcal{J}[\cdot] = d[\cdot]d^\dagger$.

2. Results

In this section, we explore how the non-Markovianity of the system-bath interactions affects the waiting time distribution, $\mathcal{W}(\mathcal{J};\tau)$. In particular, we will show the dependence of the oscillation amplitude and the spectral blue shift in the WTD as a function of Γ_L , in the short-time limit.

As shown in Fig. 9(a), oscillations in $\mathcal{W}(\mathcal{J};\tau)$ emerge and become increasingly pronounced at stronger values of Γ_L . In Fig. 9(b) we further analyze the spectral features of the WTD revealing two effects: an amplification of the oscillation amplitude and a blue shift in the oscillation frequency as Γ_L increases.

The enhancement of the oscillation amplitude likely arises from non-Markovian effects due to stronger system-bath interactions. To support this point of view, we show that, indeed, non-Markovian effects exist and become more evident as the system-bath interaction increases which also contributes to the spectral blue-shift. We do this in Fig. 10 where we plot the non-Markovianity $\mathcal{N}(\hat{\mathcal{G}})$ (which quantifies the back-flow of information from the environment to the system) as a function of Γ_L . The monotonic increase in $\mathcal{N}(\hat{\mathcal{G}})$ with Γ_L is consistent with the enhanced oscillation amplitude in the WTD, as they

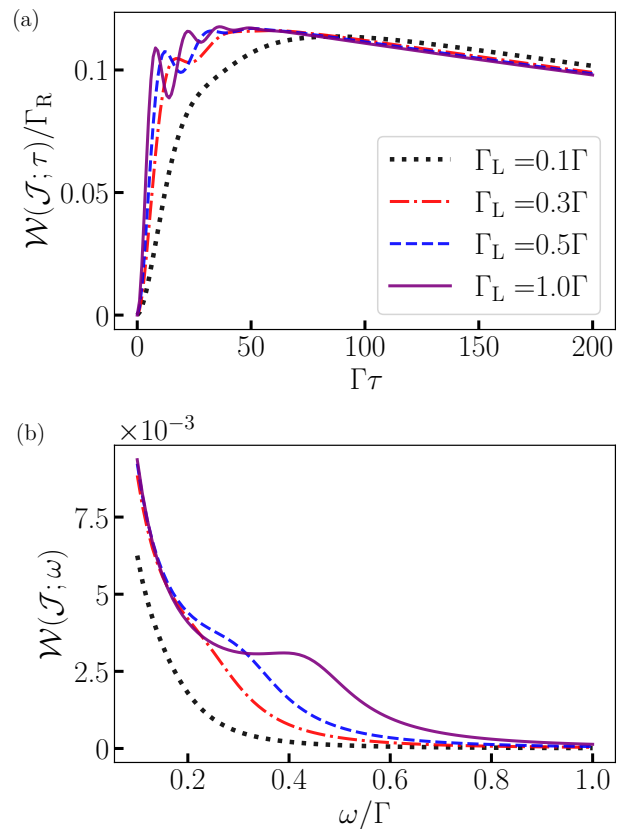


FIG. 9. (a) $\mathcal{W}(\mathcal{J};\tau)$ for different coupling strengths $\Gamma_L = 0.1, 0.3, 0.5, 1\Gamma$ to the left lead. Oscillations emerge in the short-time regime for $\Gamma_L > 0.1\Gamma$, with their frequency increasing at larger Γ_L . Here, the parameters are $\epsilon = -0.1\Gamma$, $k_B T = 0.5\Gamma$, and $W = 0.1\Gamma$. (b) Fourier-transform $\mathcal{W}(\mathcal{J};\omega)$ of the WTD. Both the amplitude of the peaks and the overall blue shift are enhanced at larger Γ_L , i.e. for stronger system-bath coupling.

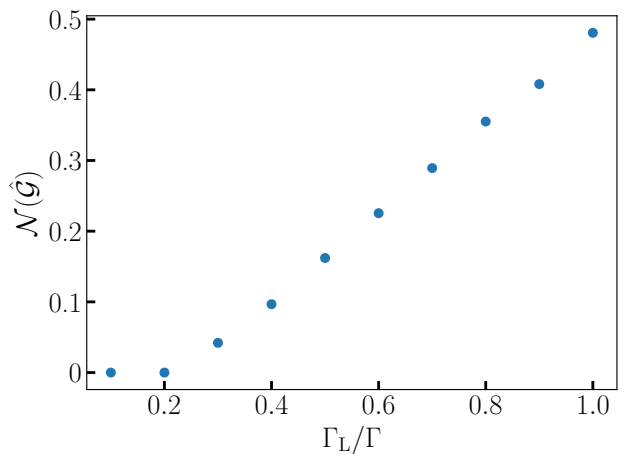


FIG. 10. Non-Markovianity $\mathcal{N}(\hat{\mathcal{G}})$ as a function of the coupling strength Γ_L to the left lead. In the single charge model considered here, $\mathcal{N}(\hat{\mathcal{G}})$ increases monotonically with Γ_L .

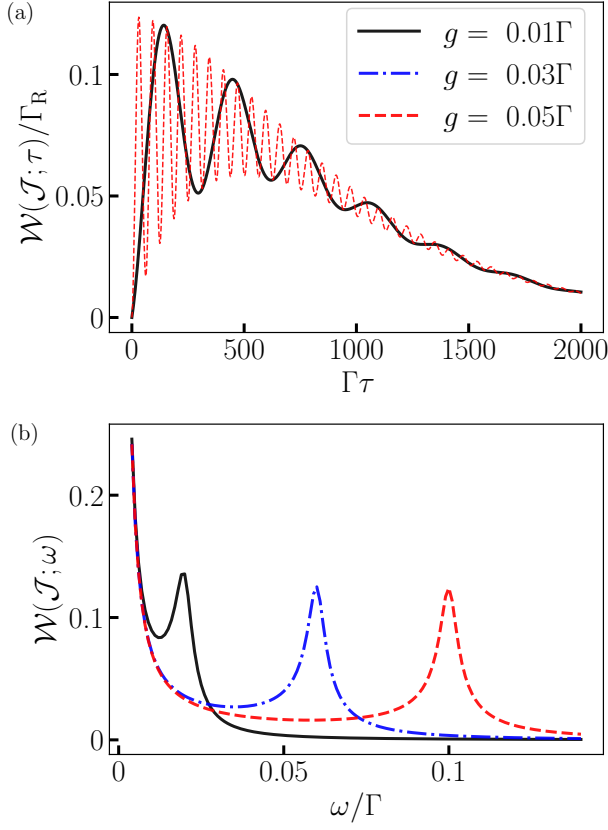


FIG. 11. WTD for a pseudo-fermion toy model. In (a) we plot $\mathcal{W}(\mathcal{J}; \tau)$, with parameters given by $\epsilon_s = \epsilon_b = -0.1\Gamma$, $W = 0.1\Gamma$, $g = 0.05\Gamma$, and $k_B T = 0.5\Gamma$. In (b) we plot the Fourier-transform $\mathcal{W}(\mathcal{J}; \omega)$, as a function of the system-(pseudo-fermion) coupling strength g . Increasing g induces a blue shift in the WTD oscillation frequency, consistently with Eq. (A4).

both originate from the presence of stronger system-bath interaction.

We are now going to present a toy model to justify these effects more in detail.

In fact, for sufficiently strong couplings, coherent effects can start to manifest in the energy exchange between the system and the bath. To model this, we are going to approximate the left lead with a pseudo-fermion coherently coupled to the system as described by the Hamiltonian

$$H_T^t = H_s^t + H_f^t + H_{sf}^t. \quad (\text{A2})$$

Here, H_s^t characterizes the system quantum dot, H_f^t describes both the pseudo-fermion (modeling the left lead) and the right lead (acting as a detector), and H_{sf}^t is the interaction Hamiltonian between the system and both leads.

These Hamiltonians are specifically defined as follows

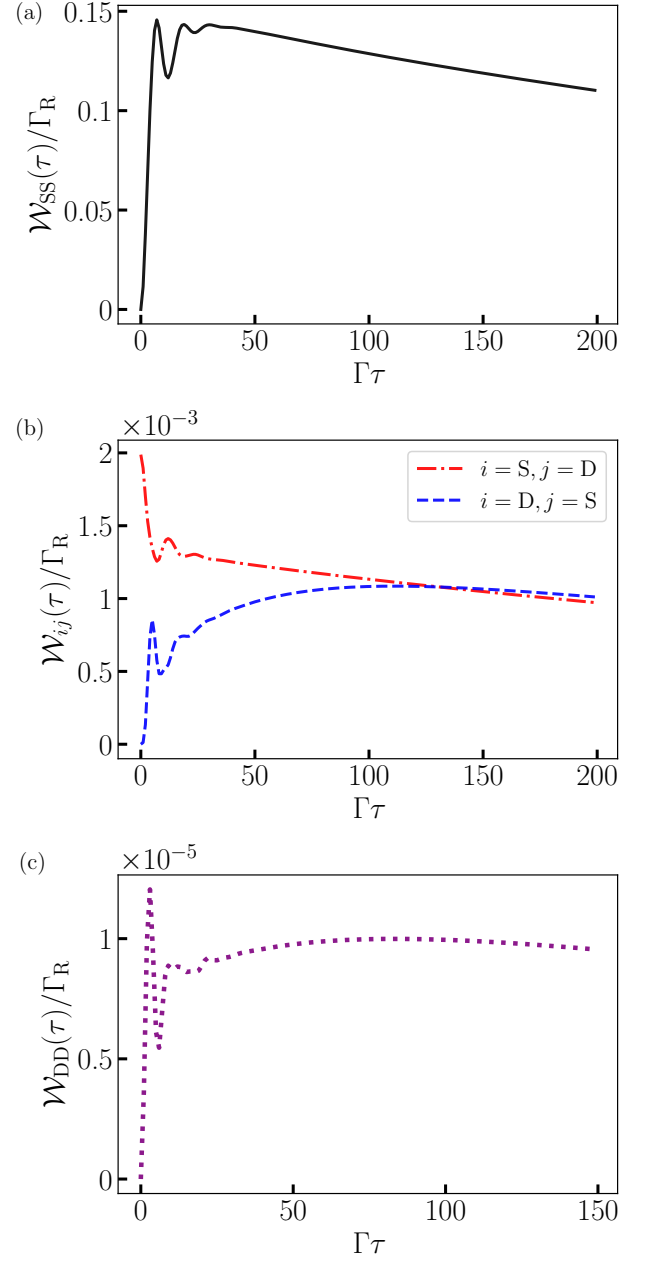


FIG. 12. Contributions from two subsequent jumps \mathcal{J}_i and \mathcal{J}_j in $\mathcal{W}(\mathcal{J}; \tau)$. (a) the scale of $\mathcal{W}_{SS}(\tau)$ shows that the value of $\mathcal{W}(\mathcal{J}; \tau)$ is dominated by contributions from events involving two \mathcal{J}_S jumps. (b) Here, we plot the contributions from different jump events, i.e., for \mathcal{J}_i and \mathcal{J}_j with $i \neq j$. We note that $\mathcal{W}_{SD}(\tau = 0)$ is non-zero since $\text{Tr}[\mathcal{J}_S \mathcal{J}_D \rho_{st}] \neq 0$ allowing two electrons to jump at the same time. On the other hand, $\text{Tr}[\mathcal{J}_D \mathcal{J}_S \rho_{st}] = 0$, which implies that $\mathcal{W}_{DS}(\tau = 0) = 0$. (c) $\mathcal{W}_{DD}(\tau)$. Since electrons are not likely to jump from the $|\uparrow\downarrow\rangle$ state, the contribution from $\mathcal{W}_{DD}(\tau)$ is negligible compared to other double-jump events. Here, $W = 0.1\Gamma$, $\epsilon = -0.1\Gamma$, $U = 1\Gamma$, $\Gamma_L = 1\Gamma$, and $\Gamma_R = 0.01\Gamma$.

$$\begin{aligned}
H_s^t &= \epsilon_s d_s^\dagger d_s, \\
H_f^t &= \epsilon_b d_b^\dagger d_b + \sum_k \omega_k c_k^\dagger c_k, \\
H_{sf}^t &= g(d_s^\dagger d_b + d_b^\dagger d_s) + \sum_k g_k(c_k^\dagger d_s + d_s^\dagger c_k),
\end{aligned} \tag{A3}$$

in terms of the fermionic creation operators for the system $d_{i=s}^\dagger$, for the pseudo-fermion $d_{i=b}^\dagger$, and for the electrons in the right-lead c_k^\dagger . Here, g is the interaction strength between the system and the pseudo-fermion.

Interestingly, this model allows to analytically estimate the frequency of the oscillations in the WTD shown in Fig. 11(a) as

$$\frac{1}{2} \sqrt{(\gamma_e - \gamma_a)^2 - 16g^2}, \tag{A4}$$

where $\gamma_e = J_R(\epsilon)(1 - n_\alpha^{\text{eq}}(\epsilon))$ and $\gamma_a = J_R(\epsilon)n_\alpha^{\text{eq}}(\epsilon)$. In fact, Eq. A4 clearly shows the blue shift in frequency as g is increased as observed in Fig. 11(b). These findings align with the data provided in Fig. 9 to provide further evidence that strong system-bath interactions lead to the emergence of both the non-Markovian oscillations in $\mathcal{W}(\mathcal{J}; \tau)$ and the corresponding blue shift in the frequency domain.

Appendix B: Decomposition of $\mathcal{W}(\mathcal{J}; \tau)$

Here, we analyze a decomposition of the $\mathcal{W}(\mathcal{J}; \tau)$ in terms of different jump processes for the SIAM case. In fact, the full interaction operator \mathcal{J} encodes the effects of different processes such as the jumps \mathcal{J}_1 and \mathcal{J}_2 of electrons from the single occupation state and the jumps \mathcal{J}_3

and \mathcal{J}_4 of electrons from the double occupation state into a single occupied one. More specifically, we can define $\mathcal{J} = \mathcal{J}_S + \mathcal{J}_D$ in terms of $\mathcal{J}_S = \mathcal{J}_1 + \mathcal{J}_2$ and $\mathcal{J}_D = \mathcal{J}_3 + \mathcal{J}_4$ and decompose the WTD as

$$\begin{aligned}
\mathcal{W}(\mathcal{J}; \tau) &= \frac{\text{Tr} \left[(\mathcal{J}_S + \mathcal{J}_D) e^{\hat{\mathcal{M}}_0 \tau} (\mathcal{J}_S + \mathcal{J}_D) \rho_{\text{st}} \right]}{\text{Tr} [\mathcal{J} \rho_{\text{st}}]} \\
&= \mathcal{W}_{\text{SS}}(\tau) + \mathcal{W}_{\text{DD}}(\tau) + \mathcal{W}_{\text{SD}} + \mathcal{W}_{\text{DS}}(\tau),
\end{aligned} \tag{B1}$$

where

$$\mathcal{W}_{ij}(\tau) = \frac{\text{Tr} \left[\mathcal{J}_i e^{\hat{\mathcal{M}}_0 \tau} \mathcal{J}_j \rho_{\text{st}} \right]}{\text{Tr} [\mathcal{J} \rho_{\text{st}}]}. \tag{B2}$$

In other words, $\mathcal{W}_{ij}(\tau)$ characterizes the effects of the jump \mathcal{J}_j followed by the jump \mathcal{J}_i after a time τ .

We can now investigate $\mathcal{W}_{ij}(\tau)$ in the case when the impurity is at equilibrium ($\mu = 0$) in the ultra-strong coupling regime to the left lead ($\Gamma_L = 1\Gamma$) and weak coupling to the right lead ($\Gamma_R = 0.01\Gamma$). We also consider a large repulsion $U = 1\Gamma$ which implies $\text{Tr}[\mathcal{J}_S \rho_{\text{st}}] \gg \text{Tr}[\mathcal{J}_D \rho_{\text{st}}]$ and justifies the relative scales $\mathcal{W}_{\text{SS}}(\tau) \gg \mathcal{W}_{\text{SD}}(\tau), \mathcal{W}_{\text{DS}}(\tau), \mathcal{W}_{\text{DD}}(\tau)$ in Fig. 12. In fact, in this regime, processes for which an electron leaves the system are mostly determined by \mathcal{J}_S , which leads to $\mathcal{W}_{\text{SS}}(\tau) \approx \mathcal{W}(\mathcal{J}; \tau)$ in Fig. 12(a). At the same time, the fact that the jumps \mathcal{J}_D bring the system to the singly-occupied state further implies that $\text{Tr}[\mathcal{J}_S \mathcal{J}_D \rho_{\text{st}}] \neq 0$, which is manifested in the non-zero value for $\mathcal{W}_{\text{DS}}(\tau = 0)$ in Fig. 12(b). Similarly, \mathcal{J}_S characterizes jumps into the empty state, resulting in $\text{Tr}[\mathcal{J}_D \mathcal{J}_S \rho_{\text{st}}]$ and $\mathcal{W}_{\text{DS}}(\tau = 0) = 0$. Furthermore, Fig. 12(c) shows that processes which involve two consecutive jumps in \mathcal{J}_D are less likely to happen, minimizing the influence of $\mathcal{W}_{\text{DD}}(\tau)$ on $\mathcal{W}(\mathcal{J}; \tau)$.

-
- [1] H.-P. Breuer and F. Petruccione, *The Theory of Open Quantum System* (Oxford University Press on Demand, New York, 2002).
 - [2] D. Manzano, A short introduction to the Lindblad master equation, *AIP Advances* **10**, 025106 (2020).
 - [3] E. Davies, *Quantum Theory of Open Systems* (Academic Press, London, 1976).
 - [4] H. Carmichael, *An Open Systems Approach to Quantum Optics* (Springer-Verlag, Berlin, 1991).
 - [5] H.-P. Breuer and F. Petruccione, *The Theory of Open Quantum Systems* (Oxford University Press, New York, 2007).
 - [6] B.-H. Liu, L. Li, Y.-F. Huang, C.-F. Li, G.-C. Guo, E.-M. Laine, H.-P. Breuer, and J. Piilo, Experimental control of the transition from markovian to non-markovian dynamics of open quantum systems, *Nat. Phys.* **7**, 931–934 (2011).
 - [7] W.-M. Zhang, P.-Y. Lo, H.-N. Xiong, MatisseWei-Yuan Tu, and F. Nori, General Non-Markovian Dynamics of Open Quantum Systems, *Phys. Rev. Lett.* **109**, 170402 (2012).
 - [8] H.-N. Xiong, P.-Y. Lo, W.-M. Zhang, D. H. Feng, and F. Nori, Non-Markovian Complexity in the Quantum-to-Classical Transition, *Sci. Rep.* **5**, 13353 (2015).
 - [9] H.-P. Breuer, E.-M. Laine, J. Piilo, and B. Vacchini, Colloquium: Non-Markovian dynamics in open quantum systems, *Rev. Mod. Phys.* **88**, 021002 (2016).
 - [10] I. de Vega and D. Alonso, Dynamics of non-Markovian open quantum systems, *Rev. Mod. Phys.* **89**, 015001 (2017).
 - [11] M. M. Wolf, J. Eisert, T. S. Cubitt, and J. I. Cirac, Assessing Non-Markovian Quantum Dynamics, *Phys. Rev. Lett.* **101**, 150402 (2008).
 - [12] H.-P. Breuer, E.-M. Laine, and J. Piilo, Measure for the Degree of Non-Markovian Behavior of Quantum Processes in Open Systems, *Phys. Rev. Lett.* **103**, 210401 (2009).
 - [13] E.-M. Laine, J. Piilo, and H.-P. Breuer, Measure for the

- non-Markovianity of quantum processes, *Phys. Rev. A* **81**, 062115 (2010).
- [14] F. Liu, X. Zhou, and Z.-W. Zhou, Memory effect and non-Markovian dynamics in an open quantum system, *Phys. Rev. A* **99**, 052119 (2019).
- [15] A. Braggio, J. König, and R. Fazio, Full Counting Statistics in Strongly Interacting Systems: Non-Markovian Effects, *Phys. Rev. Lett.* **96**, 026805 (2006).
- [16] C. Flindt, T. Novotný, A. Braggio, M. Sassetti, and A.-P. Jauho, Counting Statistics of Non-Markovian Quantum Stochastic Processes, *Phys. Rev. Lett.* **100**, 150601 (2008).
- [17] G. Schaller, G. Kießlich, and T. Brandes, Transport statistics of interacting double dot systems: Coherent and non-Markovian effects, *Phys. Rev. B* **80**, 245107 (2009).
- [18] S. V. Moreira, B. Marques, R. R. Paiva, L. S. Cruz, D. O. Soares-Pinto, and F. L. Semião, Enhancing quantum transport efficiency by tuning non-Markovian dephasing, *Phys. Rev. A* **101**, 012123 (2020).
- [19] B. Bellomo, R. Lo Franco, and G. Compagno, Non-Markovian Effects on the Dynamics of Entanglement, *Phys. Rev. Lett.* **99**, 160502 (2007).
- [20] A. Rivas, S. F. Huelga, and M. B. Plenio, Entanglement and Non-Markovianity of quantum evolutions, *Phys. Rev. Lett.* **105**, 050403 (2010).
- [21] S. Cialdi, D. Brivio, E. Tesio, and M. G. A. Paris, Programmable entanglement oscillations in a non-markovian channel, *Phys. Rev. A* **83**, 042308 (2011).
- [22] S. F. Huelga, A. Rivas, and M. B. Plenio, Non-markovianity-assisted steady state entanglement, *Phys. Rev. Lett.* **108**, 160402 (2012).
- [23] J.-S. Xu, K. Sun, C.-F. Li, X.-Y. Xu, G.-C. Guo, E. Andersson, and R. L. Franco, Experimental recovery of quantum correlations in absence of system-environment back-action, *Nat Commun* **4**, 2851 (2013).
- [24] A. Orioux, A. D'Arrigo, G. Ferranti, R. L. Franco, G. Benenti, E. Paladino, G. Falci, F. Sciarrino, and P. Mataloni, Experimental on-demand recovery of entanglement by local operations within non-markovian dynamics, *Sci Rep* **5**, 8575 (2015).
- [25] L. Kouwenhoven and L. Glazman, Revival of the Kondo effect, *Phys. World* **14**, 33 (2001).
- [26] S. Y. Cho and R. H. McKenzie, Quantum entanglement in the two-impurity kondo model, *Phys. Rev. A* **73**, 012109 (2006).
- [27] L. Amico, R. Fazio, A. Osterloh, and V. Vedral, Entanglement in many-body systems, *Rev. Mod. Phys.* **80**, 517 (2008).
- [28] I. Affleck, N. Laflorencie, and E. S. Sørensen, Entanglement entropy in quantum impurity systems and systems with boundaries, *J. Phys. A: Math. Theor.* **42**, 504009 (2009).
- [29] S.-S. B. Lee, J. Park, and H.-S. Sim, Macroscopic Quantum Entanglement of a Kondo Cloud at Finite Temperature, *Phys. Rev. Lett.* **114**, 057203 (2015).
- [30] C. Wagner, T. Chowdhury, J. H. Pixley, and K. Ingersent, Long-Range Entanglement near a Kondo-Destruction Quantum Critical Point, *Phys. Rev. Lett.* **121**, 147602 (2018).
- [31] D. Kim, J. Shim, and H.-S. Sim, Universal Thermal Entanglement of Multichannel Kondo Effects, *Phys. Rev. Lett.* **127**, 226801 (2021).
- [32] P.-C. Kuo, N. Lambert, M. Cirio, Y.-T. Huang, F. Nori, and Y.-N. Chen, Kondo QED: The Kondo effect and photon trapping in a two-impurity Anderson model ultrastrongly coupled to light, *Phys. Rev. Res.* **5**, 043177 (2023).
- [33] D. Sprinzak, Y. Ji, M. Heiblum, D. Mahalu, and H. Shtrikman, Charge Distribution in a Kondo-Correlated Quantum Dot, *Phys. Rev. Lett.* **88**, 176805 (2002).
- [34] M. Avinun-Kalish, M. Heiblum, A. Silva, D. Mahalu, and V. Umansky, Controlled Dephasing of a Quantum Dot in the Kondo Regime, *Phys. Rev. Lett.* **92**, 156801 (2004).
- [35] M. Pustilnik and L. Glazman, Kondo effect in quantum dots, *J. Phys.: Condens. Matter* **16**, R513 (2004).
- [36] A. J. Keller, S. Amasha, I. Weymann, C. P. Moca, I. G. Rau, J. A. Katine, H. Shtrikman, G. Zaránd, and D. Goldhaber-Gordon, Emergent SU(4) Kondo physics in a spin-charge-entangled double quantum dot, *Nat. Phys.* **10**, 145–150 (2014).
- [37] K. Le Hur, Quantum dots and the Kondo effect, *Nature* **526**, 203–204 (2015).
- [38] R.-N. Shang, T. Zhang, G. Cao, H.-O. Li, M. Xiao, G.-C. Guo, and G.-P. Guo, Direct observation of the orbital spin kondo effect in gallium arsenide quantum dots, *Phys. Rev. B* **97**, 085307 (2018).
- [39] H. Jeong, A. M. Chang, and M. R. Melloch, The Kondo Effect in an Artificial Quantum Dot Molecule, *Science* **293**, 2221–2223 (2001).
- [40] A. Komnik and A. O. Gogolin, Full Counting Statistics for the Kondo Dot, *Phys. Rev. Lett.* **94**, 216601 (2005).
- [41] A. O. Gogolin and A. Komnik, Towards full counting statistics for the Anderson impurity model, *Phys. Rev. B* **73**, 195301 (2006).
- [42] M. Grobis, I. G. Rau, R. M. Potok, H. Shtrikman, and D. Goldhaber-Gordon, Universal Scaling in Nonequilibrium Transport through a Single Channel Kondo Dot, *Phys. Rev. Lett.* **100**, 246601 (2008).
- [43] T. K. T. Nguyen and M. N. Kiselev, Thermoelectric Transport in a Three-Channel Charge Kondo Circuit, *Phys. Rev. Lett.* **125**, 026801 (2020).
- [44] X. Zheng, J. Jin, S. Welack, M. Luo, and Y. Yan, Numerical approach to time-dependent quantum transport and dynamical Kondo transition, *J. Chem. Phys.* **130**, 164708 (2009).
- [45] M. Schiro and O. Scarlatella, Quantum impurity models coupled to Markovian and non-Markovian baths, *J. Chem. Phys.* **151**, 044102 (2019).
- [46] G.-M. Tang and J. Wang, Full-counting statistics of charge and spin transport in the transient regime: A nonequilibrium green's function approach, *Phys. Rev. B* **90**, 195422 (2014).
- [47] T. Brandes, Waiting times and noise in single particle transport, *Ann. Phys. (Berlin)* **520**, 477 (2008).
- [48] S. Welack, M. Esposito, U. Harbola, and S. Mukamel, Interference effects in the counting statistics of electron transfers through a double quantum dot, *Phys. Rev. B* **77**, 195315 (2008).
- [49] S. Welack, S. Mukamel, and Y. Yan, Waiting time distributions of electron transfers through quantum dot Aharonov-Bohm interferometers, *Europhys. Lett.* **85**, 57008 (2009).
- [50] S. Welack and Y. Yan, Non-Markovian theory for the waiting time distributions of single electron transfers, *J. Chem. Phys.* **131**, 114111 (2009).
- [51] K. H. Thomas and C. Flindt, Electron waiting times

- in non-Markovian quantum transport, *Phys. Rev. B* **87**, 121405(R) (2013).
- [52] G.-M. Tang, F. Xu, and J. Wang, Waiting time distribution of quantum electronic transport in the transient regime, *Phys. Rev. B* **89**, 205310 (2014).
- [53] B. Sothmann, Electronic waiting-time distribution of a quantum-dot spin valve, *Phys. Rev. B* **90**, 155315 (2014).
- [54] V. Talbo, J. Mateos, S. Retailleau, P. Dollfus, and T. González, Time-dependent shot noise in multi-level quantum dot-based single-electron devices, *Semicond. Sci. Technol.* **30**, 055002 (2015).
- [55] S. L. Rudge and D. S. Kosov, Distribution of residence times as a marker to distinguish different pathways for quantum transport, *Phys. Rev. E* **94**, 042134 (2016).
- [56] S. L. Rudge and D. S. Kosov, Distribution of tunnelling times for quantum electron transport, *J. Chem. Phys.* **144**, 124105 (2016).
- [57] K. Ptaszyński, Nonrenewal statistics in transport through quantum dots, *Phys. Rev. B* **95**, 045306 (2017).
- [58] S. L. Rudge and D. S. Kosov, Distribution of waiting times between electron cotunneling events, *Phys. Rev. B* **98**, 245402 (2018).
- [59] P. Stegmann, J. König, and S. Weiss, Coherent dynamics in stochastic systems revealed by full counting statistics, *Phys. Rev. B* **98**, 035409 (2018).
- [60] E. Kleinherbers, P. Stegmann, and J. König, Revealing attractive electron–electron interaction in a quantum dot by full counting statistics, *New J. Phys.* **20**, 073023 (2018).
- [61] G. Tang, F. Xu, S. Mi, and J. Wang, Spin-resolved electron waiting times in a quantum-dot spin valve, *Phys. Rev. B* **97**, 165407 (2018).
- [62] S. L. Rudge and D. S. Kosov, Nonrenewal statistics in quantum transport from the perspective of first-passage and waiting time distributions, *Phys. Rev. B* **99**, 115426 (2019).
- [63] E. Kleinherbers, P. Stegmann, and J. König, Synchronized coherent charge oscillations in coupled double quantum dots, *Phys. Rev. B* **104**, 165304 (2021).
- [64] P. Stegmann, B. Sothmann, J. König, and C. Flindt, Electron Waiting Times in a Strongly Interacting Quantum Dot: Interaction Effects and Higher-Order Tunneling Processes, *Phys. Rev. Lett.* **127**, 096803 (2021).
- [65] W. Fu, S.-S. Ke, Y. Guo, H.-W. Zhang, and H.-F. Lü, Waiting time distribution and current correlations via a majorana single-charge transistor, *Phys. Rev. B* **106**, 075404 (2022).
- [66] E. Kleinherbers, A. Schünemann, and J. König, Full counting statistics in a majorana single-charge transistor, *Phys. Rev. B* **107**, 195407 (2023).
- [67] J. Hu, M. Luo, F. Jiang, R.-X. Xu, and Y. Yan, Padé spectrum decompositions of quantum distribution functions and optimal hierarchical equations of motion construction for quantum open systems, *J. Chem. Phys.* **134**, 244106 (2011).
- [68] Y.-T. Huang, P.-C. Kuo, N. Lambert, M. Cirio, S. Cross, S.-L. Yang, F. Nori, and Y.-N. Chen, An efficient julia framework for hierarchical equations of motion in open quantum systems, *Commun Phys* **6**, 313 (2023).
- [69] Z. H. Li, N. H. Tong, X. Zheng, D. Hou, J. H. Wei, J. Hu, and Y. J. Yan, Hierarchical Liouville-space Approach for Accurate and Universal Characterization of Quantum Impurity Systems, *Phys. Rev. Lett.* **109**, 266403 (2012).
- [70] N. Lambert, T. Raheja, S. Cross, P. Mencil, S. Ahmed, A. Pitchford, D. Burgarth, and F. Nori, QuTiP-BoFiN: A bosonic and fermionic numerical hierarchical-equations-of-motion library with applications in light-harvesting, quantum control, and single-molecule electronics, *Phys. Rev. Res.* **5**, 013181 (2023).
- [71] Y. Tanimura, Numerically “exact” approach to open quantum dynamics: The hierarchical equations of motion (HEOM), *J. Chem. Phys.* **153**, 020901 (2020).
- [72] F. Beaudoin, J. M. Gambetta, and A. Blais, Dissipation and ultrastrong coupling in circuit QED, *Phys. Rev. A* **84**, 043832 (2011).
- [73] L. Rajabi, C. Pörtl, and M. Governale, Waiting time distributions for the transport through a quantum-dot tunnel coupled to one normal and one superconducting lead, *Phys. Rev. Lett.* **111**, 067002 (2013).
- [74] K. Wrześniewski and I. Weymann, Current cross-correlations and waiting time distributions in andreev transport through cooper pair splitters based on a triple quantum dot system, *Phys. Rev. B* **101**, 155409 (2020).
- [75] K. Ptaszyński, Waiting time distribution revealing the internal spin dynamics in a double quantum dot, *Phys. Rev. B* **96**, 035409 (2017).
- [76] N. Roch, S. Florens, T. A. Costi, W. Wernsdorfer, and F. Balestro, Observation of the Underscreened Kondo effect in a Molecular Transistor, *Phys. Rev. Lett.* **103**, 197202 (2009).
- [77] M. Cirio, P. C. Kuo, Y. N. Chen, F. Nori, and N. Lambert, Canonical derivation of the fermionic influence superoperator, *Phys. Rev. B* **105**, 035121 (2022).
- [78] T. A. Costi, Kondo Effect in a Magnetic Field and the Magnetoresistivity of Kondo Alloys, *Phys. Rev. Lett.* **85**, 1504 (2000).
- [79] W. Liang, M. P. Shores, M. Bockrath, J. R. Long, and H. Park, Kondo resonance in a single-molecule transistor, *Nature* **417**, 725 (2002).
- [80] Y.-h. Zhang, S. Kahle, T. Herden, C. Stroh, M. Mayor, U. Schlickum, M. Ternes, P. Wahl, and K. Kern, Temperature and magnetic field dependence of a kondo system in the weak coupling regime, *Nat. Commun* **4**, 2110 (2013).
- [81] K. Nagaoka, T. Jamneala, M. Grobis, and M. F. Crommie, Temperature Dependence of a Single Kondo Impurity, *Phys. Rev. Lett.* **88**, 077205 (2002).
- [82] Y. Cheng, W. Hou, Y. Wang, Z. Li, J. Wei, and Y. Yan, Time-dependent transport through quantum-impurity systems with kondo resonance, *New J. Phys.* **17**, 033009 (2015).
- [83] H. Shiono, S. Ishihara, K. Mimura, H. Sato, E. F. Schwier, K. Shimada, M. Taniguchi, S.-i. Ideta, K. Tanaka, T. Zhuang, K. T. Matsumoto, K. Hiraoka, and H. Anzai, Temperature dependence of the kondo resonance peak in photoemission spectra of YbCdCu₄, *AIP Conf. Proc.* **2054**, 040013 (2019).
- [84] M. Cirio, N. Lambert, P. Liang, P.-C. Kuo, Y.-N. Chen, P. Mencil, K. Funo, and F. Nori, Pseudofermion method for the exact description of fermionic environments: From single-molecule electronics to the kondo resonance, *Phys. Rev. Res.* **5**, 033011 (2023).
- [85] F. Brange, P. Mencil, and C. Flindt, Photon counting statistics of a microwave cavity, *Phys. Rev. B* **99**, 085418 (2019).